The International Journal of Advanced Manufacturing Technology (2022) 118:1061–1076
https://doi.org/10.1007/s00170-021-08006-1

ORIGINAL ARTICLE

Study on ultrasonic-assisted WECDM of quartz wafer with continuous electrolyte flow

Chun-Hao Yang [1] · Hai-Ping Tsui [1]

Received: 30 June 2021 / Accepted: 2 September 2021 / Published online: 13 September 2021

Abstract

This study presents a novel structure for electrochemical discharge machining (WECDM) of nonconductive quartz wafers with continuous electrolyte flow. A small and stable insulating gas film was formed in the gap between the wire electrode and workpiece to achieve improved WECDM in a small area. A pulsed power supply and ultrasonic-assisted processing were combined to machine the quartz workpiece. This approach can considerably reduce unstable discharge phenomena and discharge heat generation. Furthermore, it can avoid easy breakage and subsequent loss of the wire electrode. The machining accuracy and the machining speed can be improved using appropriate WECDM parameters. Experimental results revealed that a minimum slot width of 0.208 mm was obtained at a voltage of 44 V, duration time of 100 μs, duty factor of 40%, feed rate of 20 μm/s, and ultrasonic power level of 2. Accordingly, the proposed design can obtain a smaller slot width, which improves processing accuracy.

Keywords WECDM · Pulsed power assistance · Ultrasonic assistance · Quartz · Continuous electrolyte flow

1 Introduction

The increasing demand for 5G communication and Internet of Things systems has stimulated research into materials that are used in such systems. Quartz is a key material for such systems because of its piezoelectric properties, small temperature coefficient, excellent chemical stability, and unique optical properties. To satisfy the specific functions of various components, a quartz material is typically cut into small parts or fabricated into two-dimensional or three-dimensional microstructures such as micro-holes and micro-slots. Because of the rapid miniaturization of quartz wafers, the development of innovative wafer-cutting techniques is imperative. Quartz products, such as quartz oscillators, are expected to be processed with improving quality and reducing production costs and processing times. For this reason, the scale of microfabrication of thin quartz wafers is expected to increase considerably. However, the use of conventional methods for machining quartz materials, especially in micro-fabrication, is difficult because of the hardness and brittleness of such materials. Existing wafer-cutting systems were limited by the cutting edge of cutting tools. For example, if the width of the cutting edge is wide, the slot width becomes large, resulting in a substantial loss of wafer material and thus an increase in production costs for micro-quartz wafers. Accordingly, nontraditional processing methods that use heat, light, and electrical and chemical energy to remove materials were expected to become the most effective techniques for processing hard and brittle materials.

Nontraditional machining methods for nonconductive materials include electrochemical discharge machining, abrasive jet machining, water jet machining, etching machining, ultrasonic machining, and laser machining. In laser processing, a laser power system is applied to produce a high temperature to melt materials, thus removing them from the surface of the workpiece. However, the high temperature may cause residual thermal stress and material deterioration on the surface of the workpiece, which affects the quality of the processed workpiece. Furthermore, it has several limitations due to the existence of a heat-affected zone (HAZ) surrounding the cutting area [1]. Water-jet processing involves applying high-speed water jets to the workpiece for material removal. It is not limited by material conductivity, strength, or hardness.

✉ Hai-Ping Tsui
benno@ncu.edu.tw

[1] Department of Mechanical Engineering, National Central University, Chung-Li District, Taoyuan 320, Taiwan

However, the cutting slot is not so precise. Abrasive jet processing primarily entails the use of high-speed and high–pressure abrasives for material removal. This method is mainly applied for workpiece surface treatment [2]; in addition, workpiece surface needs a mask if the method is used for micro-processing or free-standing structures [3]. However, abrasive jet processing is cumbersome and generates considerable dust, which needs the suction system. Etching machining can be classified into two categories: dry etching and wet etching. Wet etching is difficult because obtaining a precise processing shape through isotropic etching is difficult. Although nonisotropic etching provides superior precision, the etching speed is slow. Moreover, etching of microstructures with large aspect ratios is particularly difficult. Ultrasonic processing is not limited by material conductivity, strength, or hardness. However, its speed is slow when used for micro-processing; tool deflection not only affects processing accuracy but may also result in the breakage of the tool. Electrochemical discharge machining (ECDM) is an emerging nontraditional processing technology that has attracted considerable attention. In this method, material removal is achieved through chemical etching executed using spark discharge to heat up the electrolyte. This method is aimed at processing nonconductive materials. ECDM is a promising method because of its excellent processing speed and flexibility.

A number of academics have done ECDM-related research. Jain et al. experimentally observed that the gas film formed by bubbles could not create an insulation that completely coats electrodes; they proposed a theoretical model to explain the experimental data [4]. Bhattacharyya et al. proposed the best parameters for processing various nonconductive materials; their experimental results revealed that various electrode geometric features were associated with obvious differences in material removal rates [5]. Yang et al. used high-speed photography to study ECDM and demonstrated that the spark-generation mechanism in ECDM involves four stages [6]. Because of the absence of discharge sparks on the top of the electrode, the surfaces of the micro-holes and the grooves were severely tapered at the entrance. However, this method engenders severe tool wear. In 2005, Wüthrich et al. performed ECDM for micro-drilling and micro-channel machining of glass materials. The experimental results revealed that the stability of the bubble-film structure was the most critical factor affecting discharge current efficiency. The discharge energy and electrolyte-cycle characteristics at various machining depths were summarized [7–9]. Kim et al. explored the effects of various voltage pulse frequencies and duty ratios on the material removal rate and tool wear in the ECDM of a Pyrex glass. According to the experimental results, more material was removed when the duty ratio was high; however, a higher duty ratio increased tool wear [10]. Yang et al. have studied the influence of various tool-electrode materials and shapes on gas film formation and processing characteristics; their results revealed that wettability is key to gas film formation and that tungsten carbide exhibited the best processing stability. A spherical tool electrode can promote the flow of electrolytes to the electrode end, increasing the processing speed and stability [11, 12]. Cao et al. proposed a hybrid micro-grinding technique comprising ECDM and polycrystalline-diamond tools. It is suggested that this technique could affect the quality and efficiency of glass-microstructure processing; they indicated that for the fabrication of 50-μm-deep micro-grooves, this technique has a total processing time of less than 30% of that of conventional grinding and can produce superior surfaces [13]. Elhami and Razfar performed ultrasonic-assisted ECDM and achieved a high material removal rate (MRR) and low overcut [14]. Singh and Dvivedi have proposed that using textured tools during micro-channeling with ECDM can improve the material removal rate and decrease surface roughness. Textured surface provides micro-gaps resulting in thin and stable gas films [15]. Singh and Dvivedi proposed that using titrated flow of electrolyte in ECDM process drilled micro through holes could form a thin and stable gas film, which could improve machining accuracy [16].

On the basis of results obtained from studies on ECDM, several scholars have proposed substituting the tool electrode with a wire, thus engendering wire ECDM (WECDM). Some scholars used immersion processing which sinks the wire electrode into electrolyte during cutting. Peng and Liao have applied traveling wire electrochemical spark machining (TW-ECSM) to process engineering ceramics, quartz, and optical glass. It is observed that the slot width increased with the voltage. Different energy density levels are required for cutting different materials [17]. Yang et al. have proposed that adding silicon carbide powder to the electrolyte can increase the critical voltage. The powder interferes with the formation of the insulating gas film, thus reducing the discharge energy and resulting in a superior slot width and surface quality [18, 19]. Liu et al. used WECDM to process a 6061 aluminum alloy; the experimental results indicated that the magnitude of the applied current is a crucial parameter for increasing the MRR [20]. Manna and Kundal performed TW-ECSM using steel wires to cut alumina ceramics, and they analyzed the MRR and processing slot width [21]. Singh et al. have studied wire breakage in WECDM and the influence of parameters on the MRR, surface roughness, and slot width. They conducted gray correlation analysis and discovered that the MRR increased with the increasing of the voltage and electrolyte concentration, and the probability of wire breakage also increased [22, 23]. Some scholars used workpiece to press the wire electrode into the electrolyte. This can avoid larger reaction area but cause in friction between the wire electrode and workpiece. However, it will let the slot curved. Mitra et al. employed TW-ECDM to cut composites' reinforced material.

They observed that the MRR increased at high voltages. Furthermore, they used artificial neural networks for quality prediction, and the prediction results agreed with the experimental results [24]. Rattan et al. have analyzed the influence of a magnetic field on TW-ECSM and found that adding a magnetic field could increase the smoothness of electrolyte flow. Setting an appropriate magnetic field could increase the MRR from 9 to 200% [25, 26]. Wang et al. used electrochemical discharge assisted diamond wire saw. The experimental result shows that MRR can be improved by electrochemical discharge assisted [27]. Wang et al. proposed an oil film-assisted WECDM. Because the oil film on the tool wire is online covered, the electrolysis occurs only where the oil film is absent [28].

In WECDM, immersion processing involves sinking a wire electrode into the electrolyte during cutting [17–23]. This processing method requires a large quantity of electrolytes, and the wire electrode reaction area is larger and breaks easily. Another method is to press the wire electrode into the electrolyte with a workpiece, which reduces the reaction area but increases friction between the wire electrode and the workpiece [24–27]. This method was simulate by COMSOL to develop the electric field distribution in Fig. 1. The wire electrode also breaks easily in the gap between the wire electrode and workpiece due to friction and discharge spark. Kumar et al. performed TW-ECDM to process quartz and used a zinc-coated brass wire as the wire electrode. The experimental results revealed that the zinc-coated brass wire could increase the MRR and reduce the probability of wire breakage; however, wires still break occasionally [29].

In this study, a dented copper structure was established on a 304 stainless steel auxiliary electrode and under a quartz test piece and wire electrode. Insulating tape was placed between the dented copper structure and the auxiliary electrode. A potassium hydroxide (KOH) electrolyte was supplied by an electrolyte supply tube. The electric field was simulated by COMSOL in Fig. 2. As compared to Fig. 1, the electric field distribution is the same; however, the reaction area is much smaller. The workpiece will have no contact with the wire electrode. This design can promote the formation of a small area and stable insulating gas film structure between the wire electrode and the quartz workpiece to create a small area conducive for WECDM. A pulsed DC power supply and ultrasonic vibrator were applied to machine a 70-μm-thick quartz wafer. This design could markedly reduce unstable discharge phenomena and discharge heat generation. There was also no friction between the wire electrode and the workpiece. Based on the above innovative design, it can avoid easy breakage of the wire electrode and loss of a considerable quantity of electrodes. The use of appropriate WECDM parameters can also improve machining accuracy and speed. Figure 3 shows the comparison of the conventional WECDM and WECDM with continuous flow. In conventional WCEDM, the bubble will accumulate at the wire electrode and the electrolyte surface [25]. The discharge spark will appear on the wire electrode that has been immersed in the electrolyte. The reaction area will be very large. The wire electrode suffers a large amount of discharge spark energy. It will cause the breakage of the wire electrode. However, excess bubbles were flushed away in the continuous flow WECDM by the electrolyte. This phenomenon facilitated to form a thin and stable gas film. Furthermore, the discharge spark will just focus on the button of the workpiece. The wire electrode did not suffer a large amount of discharge spark energy. Easy breakage and loss of the wire electrode could be avoided.

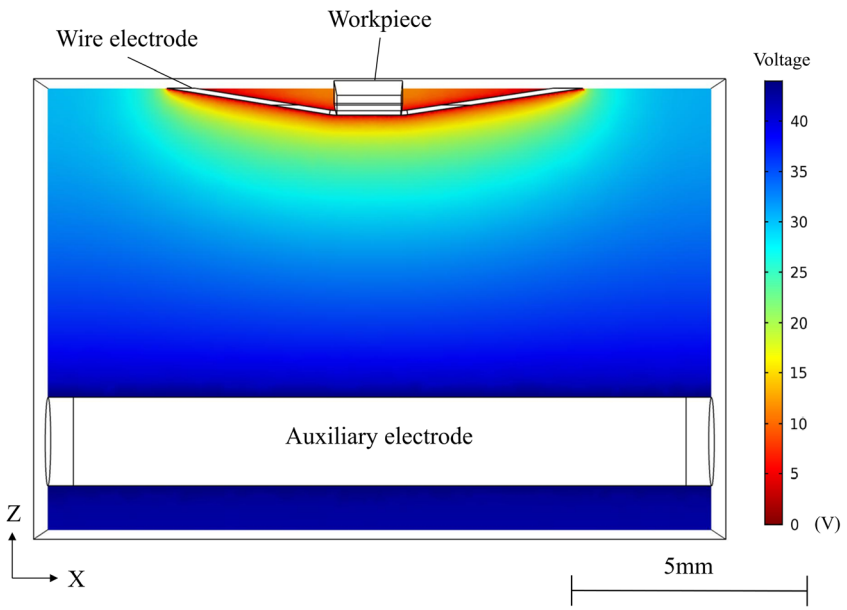

Fig. 1 Simulation of electric field distribution with contacting WECDM

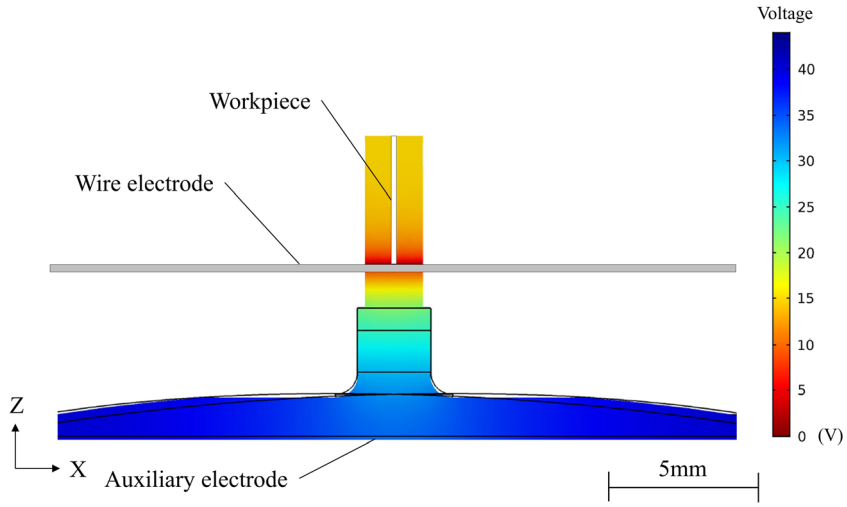

Fig. 2 Simulation of electric field distribution in this study

2 Experimental design

2.1 Experimental setup

The experimental setup is displayed in Fig. 4, and the schematic of the ultrasonic-assisted WECDM with dented copper structure is illustrated in Fig. 5. The ultrasonic vibrator was mounted on a Z-axis sliding platform with a stepping motor. A 70-μm-thick quartz workpiece was held on the copper rod, which is clamped on the ultrasonic vibrator (ACROW SL32-OLNR06-150). The dented copper structure was established on the 304 stainless steel auxiliary electrode and under the quartz test piece and wire electrode to let the electrolyte flow smoothly. Insulating tape was placed between the dented copper structure and the auxiliary electrode. Furthermore, a zinc-coated brass wire was established on a self-designed wire tension apparatus. The surface of the wire electrode was coated with zinc for

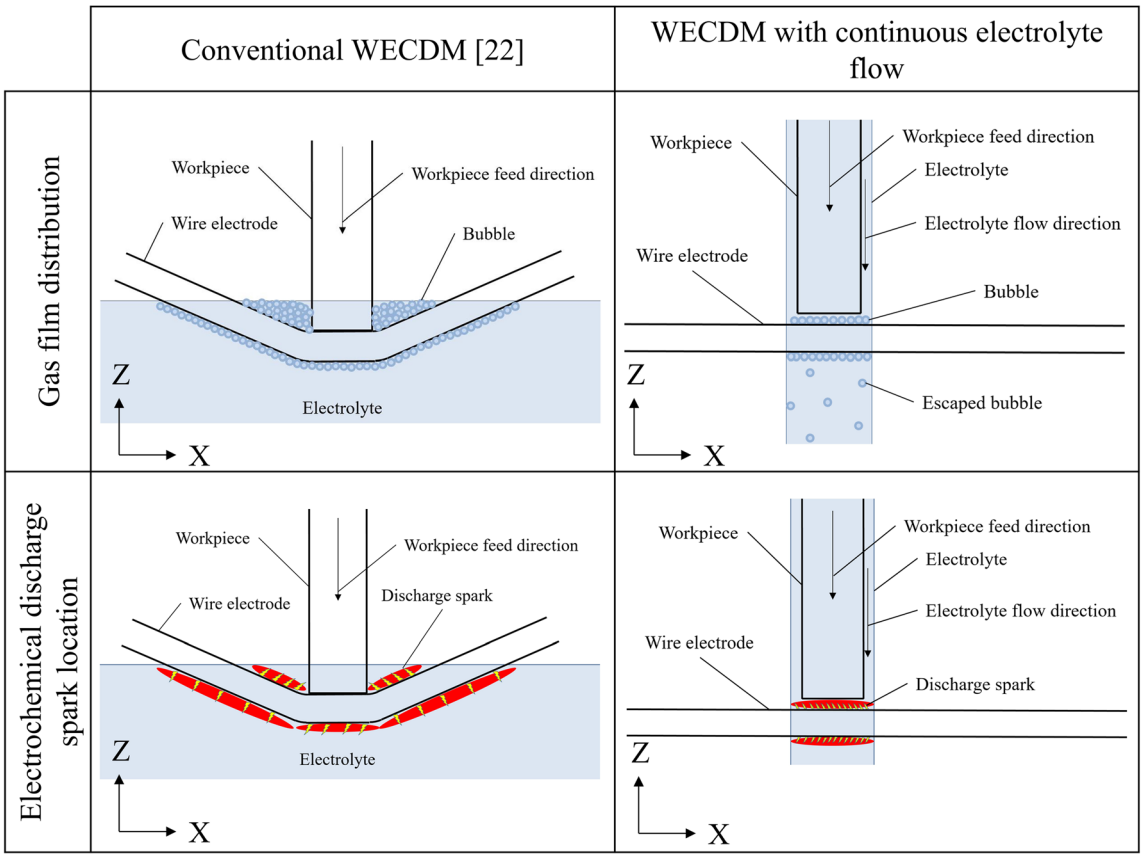

Fig. 3 Comparison of conventional WECDM and WECDM with continuous electrolyte flow

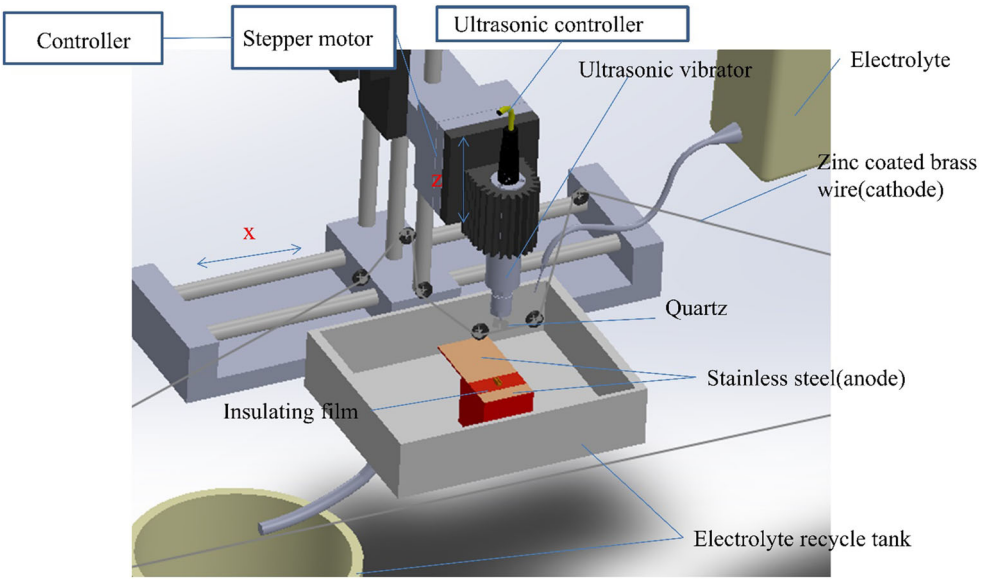

Fig. 4 Schematic of experimental setup

protection [29]. The electrolyte supply tube was used to supply KOH liquid. The pulsed power supply was connected to the zinc-coated brass wire (negative electrode) and the stainless steel auxiliary electrode (positive electrode).

In ECDM, the bubbles wrap around the wire electrode, which is produced by the electrolysis. The bubbles will form a gas film when the bubbles were more enough. The sparks will start to heat up the electrolyte when the gas film formed. The high-temperature electrolyte will accelerate the etching rate of the workpiece. According to the design of the experiment, a stable insulating gas film structure was formed between the wire electrode and the workpiece as presented in Fig. 5.

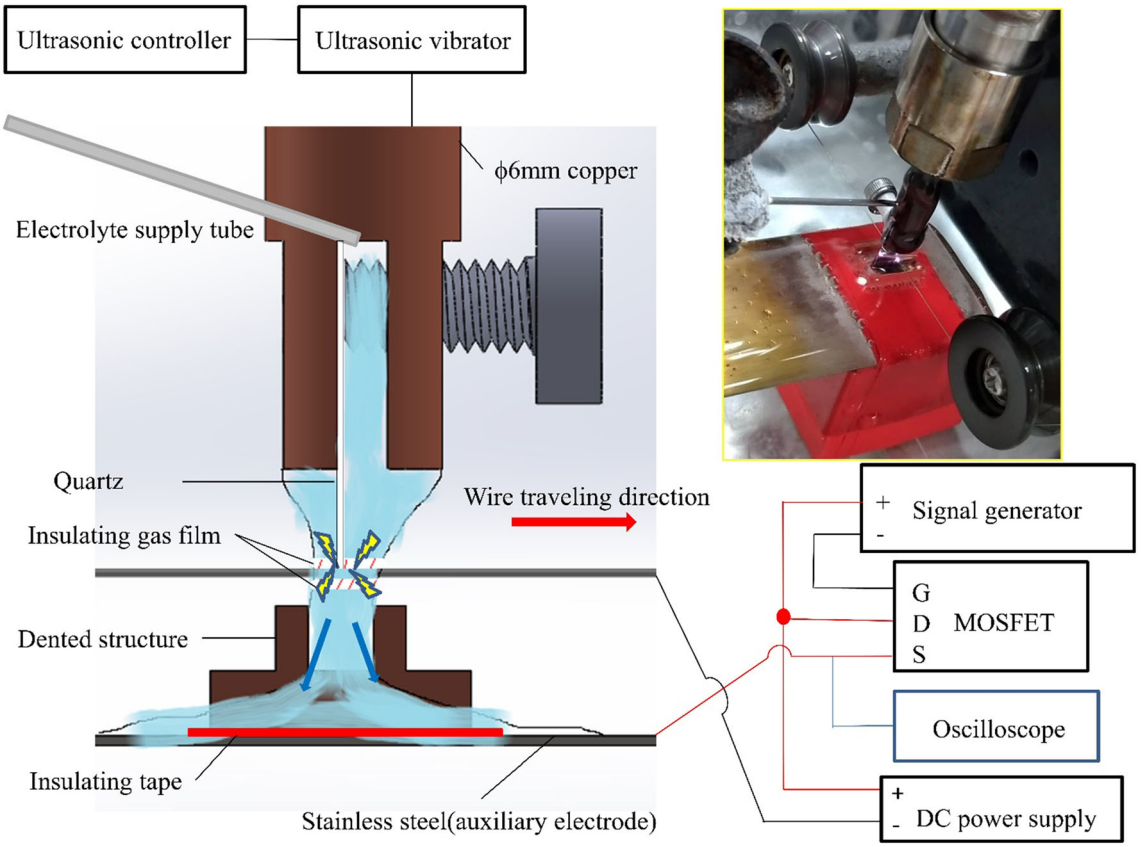

Fig. 5 Schematic of the ultrasonic-assisted WECDM

2.2 Material

Figure 6 shows the 2-in single-crystal quartz wafer with a thickness of 70 μm used in the experiment. The wafer was cut into test pieces measuring 8 mm in length and 6 mm in width.

Deionized water was mixed with KOH to obtain a 5 M electrolyte. Deionized water was used instead of tap water because tap water contains other ions that could interfere with the experiment. The auxiliary electrode was a 304-stainless steel plate with a length, width, and thickness of 60, 30, and 0.3 mm, respectively. This electrode was placed under the wire electrode (Fig. 4). A 200-μm zinc-coated brass wire was used for cutting.

2.3 Experimental method

A novel structure was created for micro-area WECDM. A pulsed DC power supply and ultrasonic-assisted vibration were applied to the structure. The experimental parameters were as follows: open voltage, processing time, duty factor, feed rate, and ultrasonic power. After the experiment, the slot widths of the quartz test pieces were measured using an optical measuring instrument. Scanning electron microscopy (SEM) was performed to observe the surface topography of the test pieces. An oscilloscope was used to measure the current value during processing. Table 1 presents parameters that were kept constant in the experiment, and Table 2 presents the variable experimental parameters. The current signal was measured by oscilloscope. The slot width was measured by optical microscope after experiment. SEM was used for observing the surface of the workpiece.

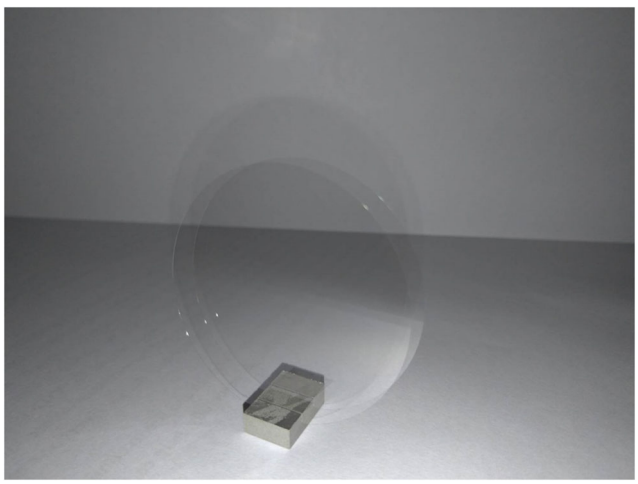

Fig. 6 Photograph of a single-crystal quartz wafer

Table 1 Constant experimental parameters

Parameter	Description
Total stroke (μm)	2000
Electrolyte	KOH (5 M)
Zinc-coated brass wire diameter (μm)	200
Initial gap (μm)	20
Ultrasonic vibration frequency (kHz)	24
Electrolyte flow rate (ml/min)	66

3 Results and discussion

3.1 Effect of open voltage on WECDM

3.1.1 Effect of open voltage on slot width for WECDM with DC power supply

The blue line in Fig. 7 illustrates the relationship between open voltage and slot width for WECDM executed with a DC power supply. The slot width increased with the open voltage increasing. A stable and thick insulating gas film formed at higher open voltages because bubbles could be easily generated at such voltages, increasing the discharge energy.

The maximum open voltage was 44 V. Any further increase in the open voltage could lead to wire breakage due to the excessive density of energy and lack of rest time.

3.1.2 Effect of open voltage on slot width for WECDM with pulsed power supply

The black line in Fig. 7 displays the relationship between the open voltage and slot width for WECDM executed using a pulsed power supply. When the open voltage was 38 V, the slot width was 0.217 mm. Moreover, when the open voltage was increased to 50 V, the slot width increased to 0.330 mm. The slot width associated with the 50 V voltage was 56.5% greater than that associated with the 38 V voltage. Further increasing the open voltage engendered the greater discharge

Table 2 Variable experimental parameters

Variable parameter	Setting value
Open voltage (V)	38, 41, 44, 47, 50
Duration time (μs)	10, 10^2, 10^3, 10^4, 10^5
Duty factor (%)	30, 40, 50, 60, 70
Feed rate (μm/s)	5, 10, 15, 20, 25
Ultrasonic power (level)	2, 4, 6, 8, 10

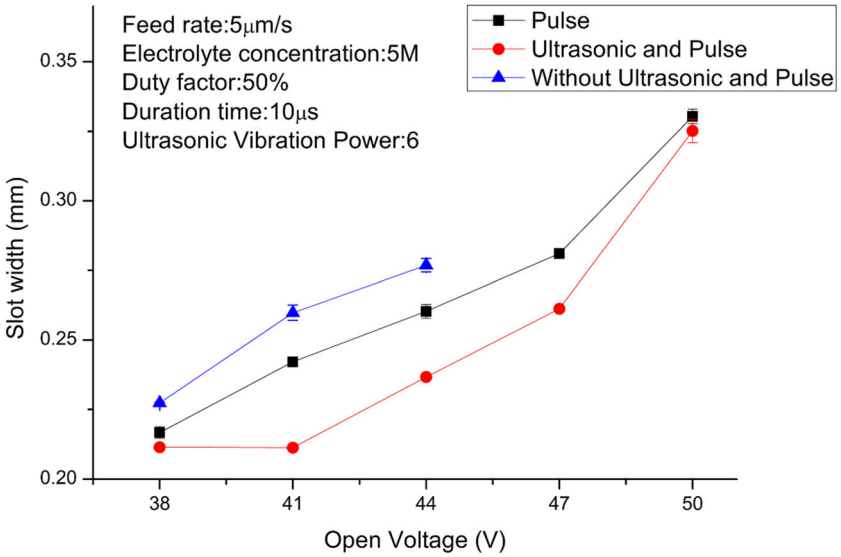

Fig. 7 Schematic of relationship between open voltage and slot width

energy. This phenomenon can result in low processing quality and large overcut.

3.1.3 Effect of open voltage on slot width for WECDM with pulsed power combined with ultrasonic assistance

An experiment was performed using pulsed power and ultrasonic vibration executed at a power level of 6. According to the red line in Fig. 7, the slot width compared with previous experiment decreases considerably as the open voltage increased from 38 to 47 V. The slot width did not decrease considerably at 50 V because of the thick gas film. The electrolysis energy generated at 50 V was so large that the thickness of the gas film was not considerably affected by ultrasonic vibration.

Figure 8 depicts an SEM image of structures processed with (Fig. 8a) or without (Fig. 8b) ultrasonic assistance. The sidewall without ultrasonic assistance was rugged and exhibited no obvious flat surface. The sidewall of the surface with ultrasonic assistance was relatively flat.

In this study, an oscilloscope was used to measure the current wave during the processing. The ultrasonic-assisted vibration drove some of the bubbles away from the bubble film, as can be seen in Fig. 9. This phenomenon could let

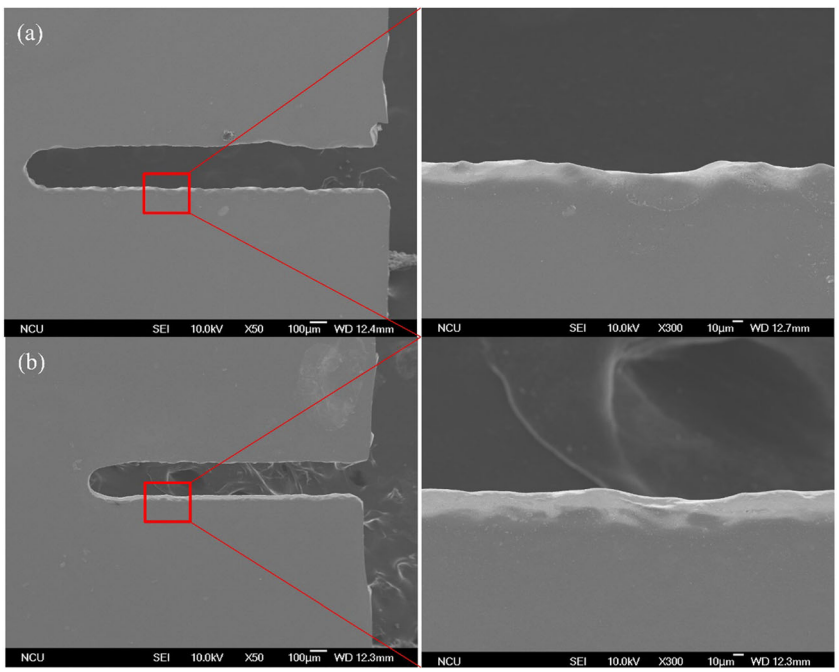

Fig. 8 SEM images of structures processed with or without ultrasonic assistance (open voltage, 44 V; duration time, 10 μs; duty factor, 50%; feed rate, 5 μm/s): **a** structure without ultrasonic assistance and **b** structure with ultrasonic assistance

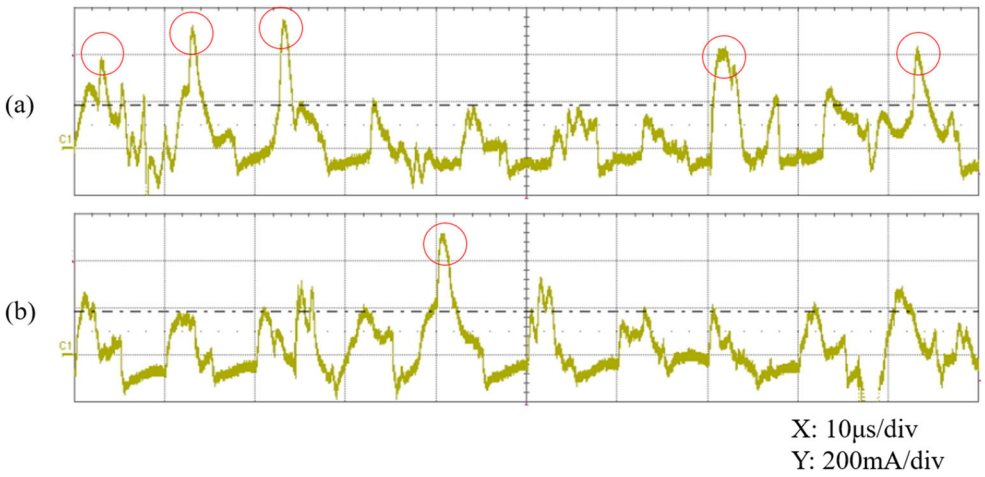

Fig. 9 Current wave diagram under 44 V in WECDM. **a** With ultrasonic assistance. **b** Without ultrasonic assistance

electrolyte contact the electrode. The electrode should form a gas film again. There have much more electrolysis current signal with ultrasonic assist compared to without ultrasonic assist. Therefore, the discharge was reduced. Figure 10 shows the photos of continuous electrolyte flow WECDM. Figure 10a shows the setup of the workpiece and the wire electrode. The wire electrode was placed under the workpiece. Figure 10b shows the WECDM without ultrasonic vibration assistance. The gas film will form around the wire electrode. The spark appears in the gas film. Figure 10c shows the WECDM with ultrasonic vibration assistance. The bubbles had been separated by ultrasonic vibration. The gas film was looser than without ultrasonic vibration. The gas film with ultrasonic vibration assistance will be thinner than the gas film without ultrasonic vibration assistance.

The schematic diagram of WECDM with ultrasonic vibration is shown in Fig. 11. The ultrasonic vibration will disturb the gas film and cause the gas film to be thinner. Therefore, the machined slot under ultrasonic vibration-assisted WECDM will be smaller. The simulation of WECDM is shown in Fig. 12. Figure 12a shows the WECDM without ultrasonic vibration assistance. The gas film is wrapped around the wire electrode. Figure 12b shows the WECDM with ultrasonic vibration assistance. The ultrasonic vibration disturbed the gas film, which causes the electric field distortion. The discharge prefers to hit the thinner gas film. The discharging gap without ultrasonic vibration assistance is thicker than the discharging gap with ultrasonic vibration assistance. Therefore, the discharge energy of WECDM with ultrasonic vibration assistance will be

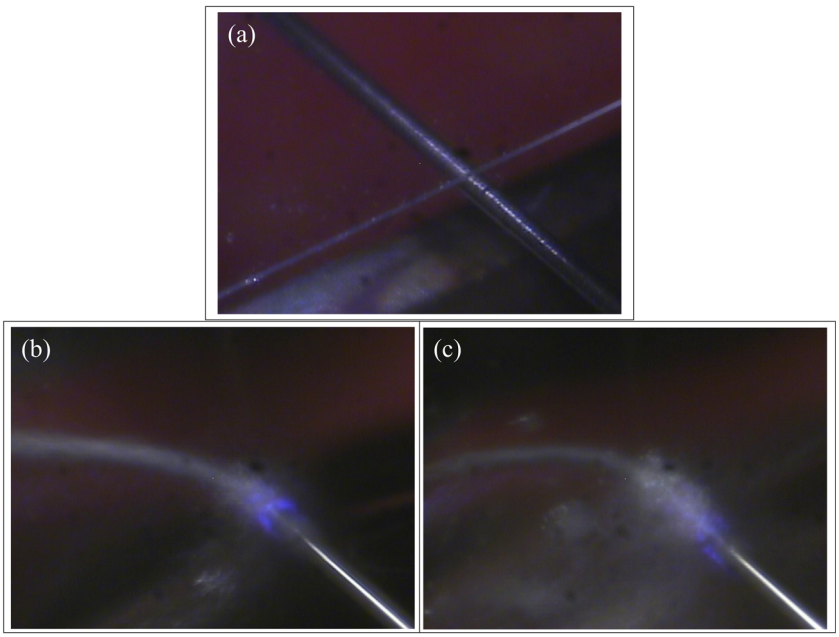

Fig. 10 Photos of continuous electrolyte flow WECDM. **a** The setup of the workpiece and the wire electrode. **b** WECDM without ultrasonic assistance. **c** WECDM with ultrasonic assistance

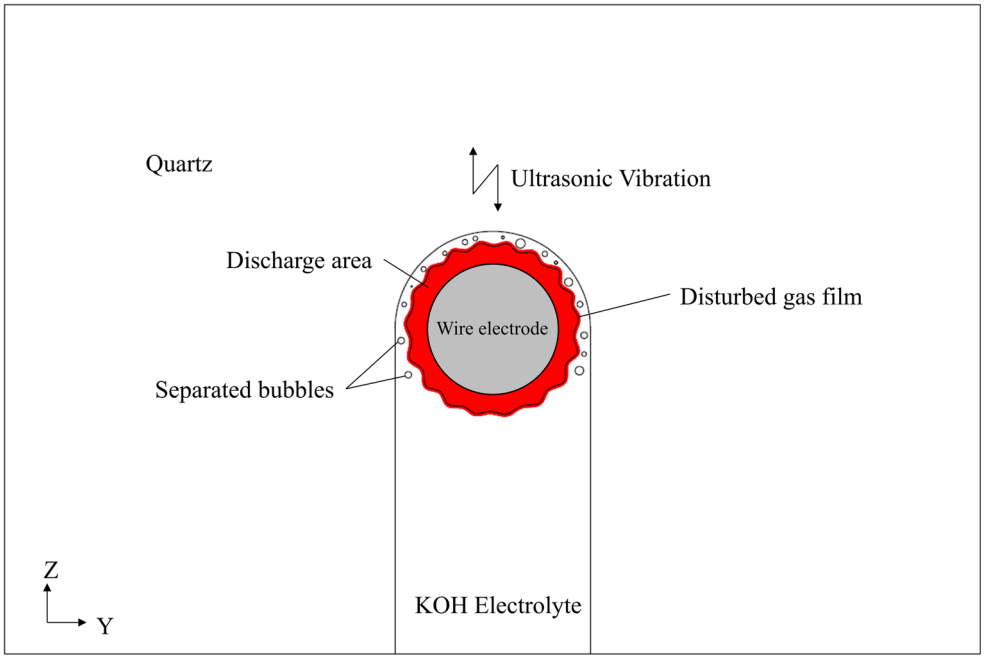

Fig. 11 Schematic diagram of WECDM with ultrasonic vibration assistance

smaller than the discharge energy without ultrasonic vibration assistance.

Figure 13 displays the current wave at various open voltages in the process executed with ultrasonic assistance. Wüthrich reported that the electrolysis current is typically more than 400 mA, which signifies that the gas film is not sufficiently stable to envelop the electrode [7]. The electrode often encounters the electrolyte, which results in a short circuit and thus generates a relatively high current. This study revealed that many electrolysis currents existed at the open voltages of 38 and 41 V (Fig. 13). By contrast, when the open voltage was 44 V, almost no electrolysis phenomenon was observed. Thus, according to the current wave diagram, the current was stable at 44 V. Accordingly, 44 V was used as the open voltage for subsequent experiments.

3.2 Effect of duration time on WECDM

3.2.1 Effect of duration time on slot width in WECDM without ultrasonic assistance

Figure 14 shows the relationship between duration time and slot width. The slot width increased with the duration time increasing (Fig. 14, black line). Discharge-induced heat accumulation also increased, leading to over corrosion and severe slot overcut. When the duration time was 100 μs, a minimum slot width of 0.249 mm was obtained. When the duration time was 100,000 μs, a maximum slot width of 0.321 mm was obtained, which was 36% larger than that obtained when the duration time was 100 μs. When the duration time was 10 μs, the slot width was 0.260 mm, which was 5.5% more than that

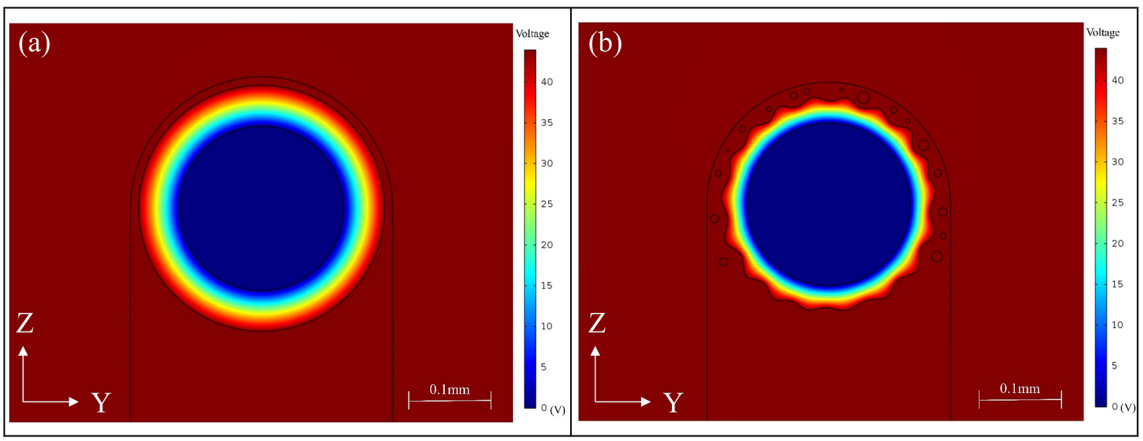

Fig. 12 The simulation of continuous electrolyte flow WECDM. **a** WECDM without ultrasonic vibration assistance. **b** WECDM with ultrasonic vibration assistance

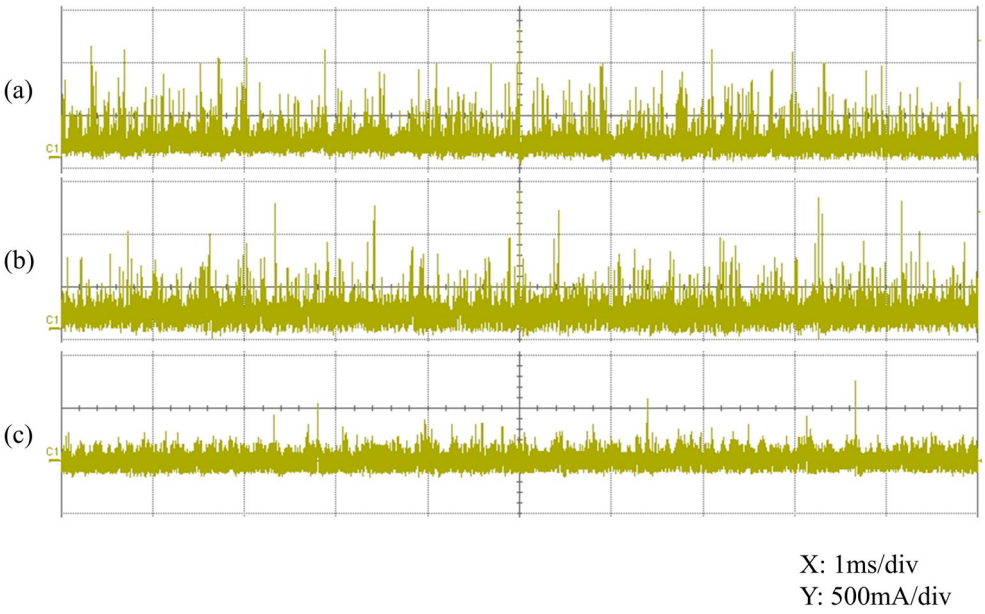

Fig. 13 Current wave diagram under various open voltages in WECDM with ultrasonic assistance: **a** 38 V, **b** 41 V, **c** 44 V

observed at 100 μs. The 10-μs time was so short that the insulating gas film continuously and steadily covered the electrode. It could be explained by the current signal (Fig. 15). In Fig. 15a, there is almost no electrolysis signal. However, there are some of the electrolysis signals in Fig. 15b. This thus obviated the necessity of reforming the gas film to induce discharge; consequently, the slot width was increased.

3.2.2 Effect of duration time on slot width in WECDM with ultrasonic assistance

The red line in Fig. 14 presents the effect of duration time on slot width in WECDM executed with ultrasonic assistance. At each duration time, the slot width observed under ultrasonic assistance was considerably smaller than that observed in machining without ultrasonic assistance because the ultrasonic vibration moved some of the bubbles away from the gas film. This phenomenon reduced the thickness of the gas film, resulting in a decrease in the slot width.

Figure 16 depicts SEM images for structures produced at various duration times with ultrasonic assistance. The side walls of the slot produced with a duration time of 100 μs are vertical and relatively flat (Fig. 16a). A fish-bone etching mark was observed on the surface of the sidewalls, which was caused by the flow of the electrolytes from left to right. The sidewall is overcut severely when the duration time is 100,000 μs (Fig. 16b). The surface of the sidewall was also jagged.

When the duration time was 100 μs, the minimum slot width was 0.222 mm. When the duration time was 100,000

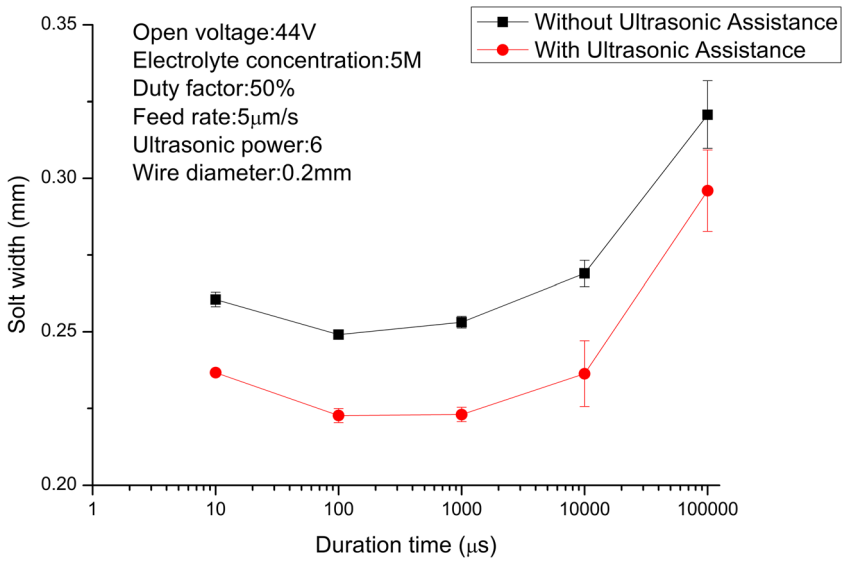

Fig. 14 Schematic of the relationship between the duration time and slot width

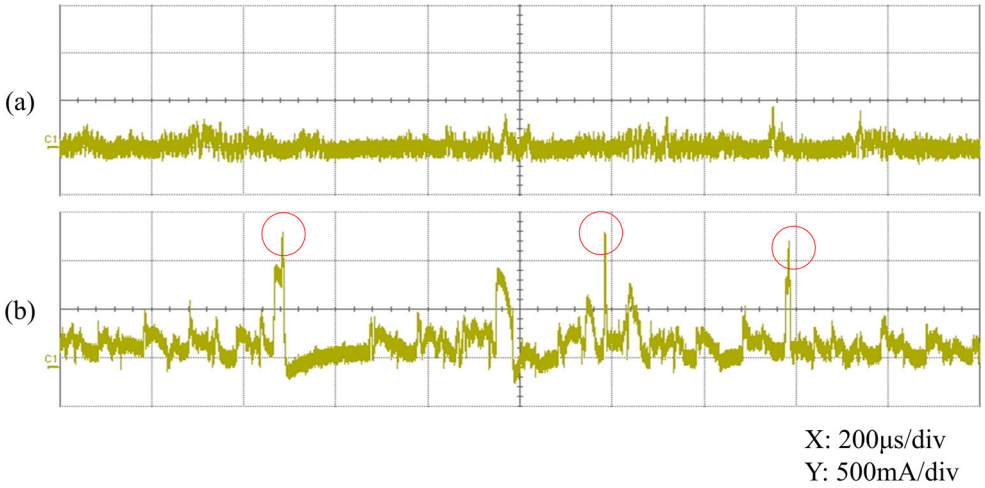

Fig. 15 Current wave diagram under different duration times in WECDM: **a** 10 μs, **b** 100 μs

μs, the maximum slot width was 0.295 mm, which was 36.5% larger than that observed at 100 μs. When the duration time was 10 μs, the slot width was 0.236 mm, which was 7% larger than that observed at 100 μs. The smallest slot width was obtained at 100 μs. Therefore, 100 μs was used as the duration time for subsequent experiments.

3.3 Effect of duty factor on WECDM

3.3.1 Effect of duty factor on slot width in WECDM without ultrasonic assistance

Figure 17 displays the relationship between duty factor and slot width. The slot width increased with the duty factor increasing (Fig. 17, black line). A high amount of energy was accumulated due to the relatively high duty factor. This resulted in the etching of the workpiece surface by hot electrolytes, thus producing a relatively large slot width [10]. When the duty factor was 30%, the smallest slot width was 0.244 mm. When the duty factor was 70%, the largest slot width was 0.261 mm, which was 10% larger than that observed at the duty factor of 30%.

3.3.2 Effect of duty factor on slot width in WECDM with ultrasonic assistance

The red line in Fig. 17 illustrates the effect of duty factor on slot width in WECDM with ultrasonic assistance. At each duty factor, the slot width observed under ultrasonic assistance was smaller than that observed in machining without

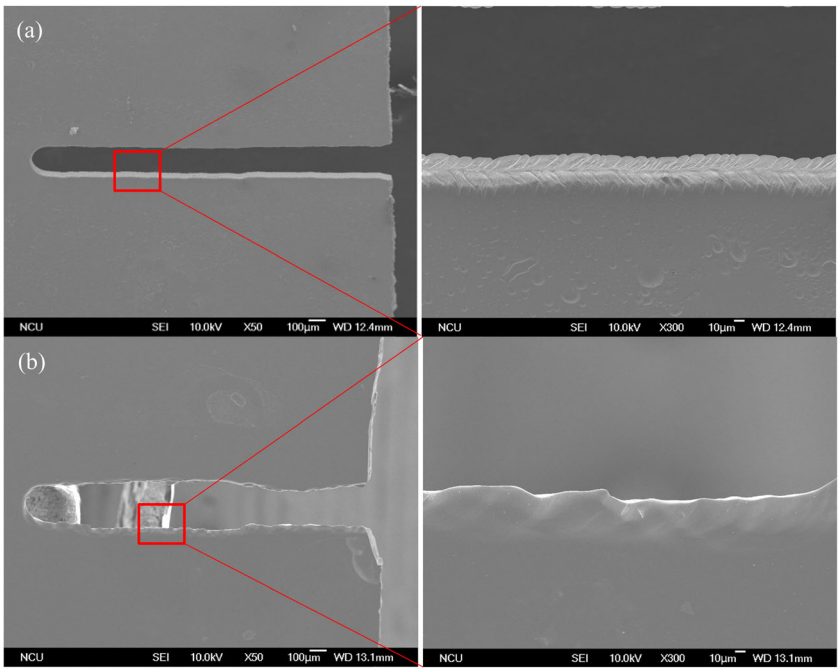

Fig. 16 SEM images of structures processed at various duration times with ultrasonic assistance (open voltage, 44 V; duty factor, 50%; feed rate, 5 μm/s; ultrasonic power level, 6): **a** duration time of 100 μs and **b** duration time of 100,000 μs

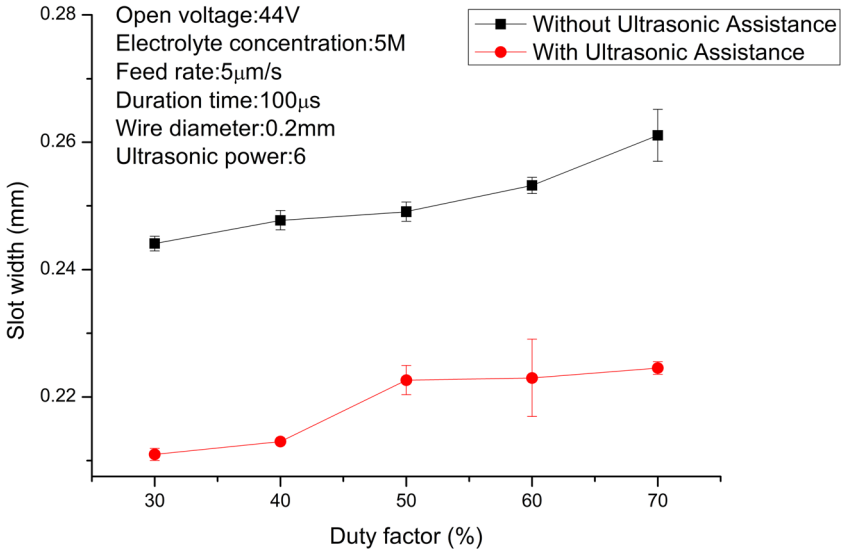

Fig. 17 Schematic of the relationship between duty factor and slot width

ultrasonic assistance. Furthermore, wire-electrode breakage was not observed in this series of experiments. When the duty factor was 30%, the smallest slot width was 0.211 mm, which was 16.5% lower than that observed in machining without ultrasonic assistance. When the duty factor was 70%, the largest slot width was 0.224 mm, which was 6.5% higher than that observed at the 30% duty factor; it was also 18.5% lower than that observed in machining without ultrasonic assistance.

However, at a duty factor of 30%, the electrochemical discharge time was short and the accumulated processing energy was low. Therefore, the etching rate could not keep up with the feed rate. The wire electrode thus rubbed against the workpiece. The low etching rate caused the wire electrode to exert excessive pressure on the workpiece, resulting in workpiece breakage. At a duty factor of 70%, the electrochemical discharge was high. Consequently, the accumulated processing energy was high, which increased the etching rate. Therefore, the slot width was relatively large.

Figure 18 depicts SEM images of structures processed at various duty factors with ultrasonic assistance. At the duty factor of 40%, the sidewalls of the slot were relatively flat and straighter than the sidewalls observed at a duty factor of 70%. Preferable processing could be achieved at the 40% duty factor. Therefore, 40% was used as the duty factor for subsequent experiments.

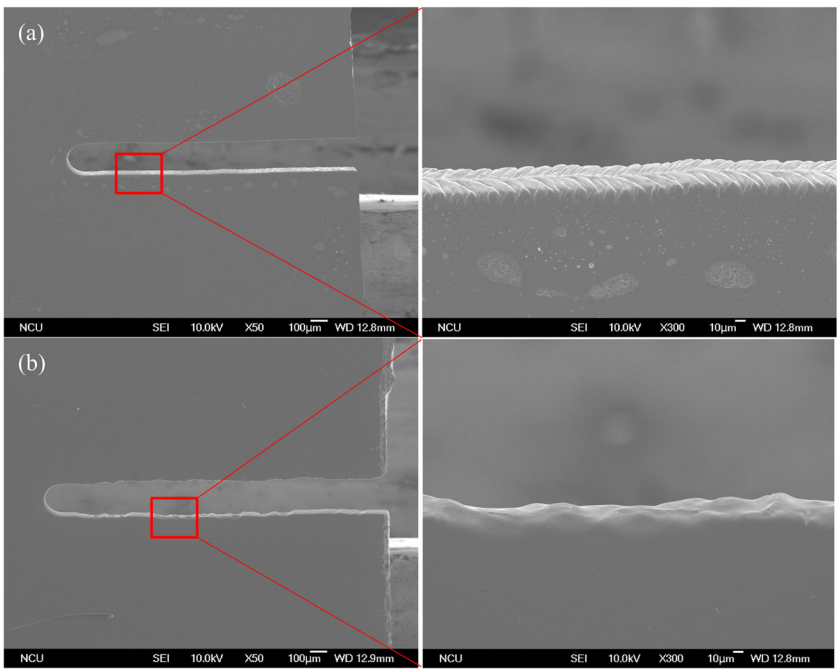

Fig. 18 SEM images of structures processed at various duty factors with ultrasonic assistance (open voltage, 44 V; duration time, 100 μs; feed rate, 5 μm/s; and ultrasonic power level, 6): **a** duty factor of 40% and **b** duty factor of 70%

3.4 Effect of feed rate on WECDM

3.4.1 Effect of feed rate on slot width in WECDM without ultrasonic assistance

Figure 19 displays the relationship between feed rate and slot width. The time for which the wire electrode remained in the same area decreased as the feed rate increased. If this time were shorter, the etching action on the slot would be lower. In WECDM without ultrasonic assistance, the largest slot width was 0.248 mm at a feed rate of 5 μm/s. The smallest slot width was 0.211 mm at a feed rate of 25 μm/s, which was 18.5% lower than that observed at 5 μm/s.

3.4.2 Effect of feed rate on slot width in WECDM with ultrasonic assistance

When ultrasonic vibration was included in the experiment, the feed rate could only be up to 20 μm/s. A feed rate higher than 20 μm/s may cause the workpiece to rupture because the etching speed cannot keep up with the feed rate, causing the wire electrode to rub against the workpiece. The wire electrode exerted excessive pressure on the workpiece, which resulted in the rupture of the workpiece. In the experiment with ultrasonic assistance, the largest slot width was 0.213 mm at a feed rate of 5 μm/s. The smallest slot width was 0.209 mm at a feed rate of 20 μm/s. The slot width obtained at 20 μm/s was reduced by 2% when compared with that obtained at 5 μm/s.

Figure 20 presents SEM of structures processed at various feed rates with ultrasonic assistance. As indicated in this figure, the etching mark on the surface of the slot sidewall decreased as the feed rate increased. When the time for which the wire electrode remained intact was shorter, the etching action on the slot was lower. Reduced etching time decreases the etching marks on the surface of the slot sidewall.

The smallest slot width was obtained at a feed rate of 20 μm/s. Therefore, 20 μm/s was used as the feed rate to perform subsequent experiments.

3.5 Effect of ultrasonic power on WECDM

Figure 21 displays the relationship between ultrasonic power and slot width. The wire electrode was not broken in this series of experiments. When the experiment was performed without ultrasonic vibration, the slot width was 0.212 mm, which was higher than that observed in the experiments performed with ultrasonic vibration. Furthermore, the slot width observed in the experiments with ultrasonic assistance increased slightly with the ultrasonic power increasing. The primary reason for this increase is that the gas film on top of the wire electrode was more likely to be disturbed by the vibration of the workpiece when the ultrasonic vibration amplitude was large. Hence, the gas film tended to be formed horizontally, and the slot width became larger. Elhami and Razfar reported that when ultrasonic vibration was applied to the electrode, the thickness of the gas film decreased. However, when the amplitude was excessively large, the horizontal gas film thickness increased [14]. The slot width was 0.211 mm when the ultrasonic power level was 10. A minimum slot width of 0.208 mm was obtained when the ultrasonic power level was 2. This slot width was 1.5% smaller than that obtained at the ultrasonic power level of 10 and was 2% smaller than that obtained in the experiments without ultrasonic assistance.

Figure 22 depicts SEM images of surface structures processed at various ultrasonic power levels. Figure 22 a displays the SEM image for the fish-bone etching mark processed at a

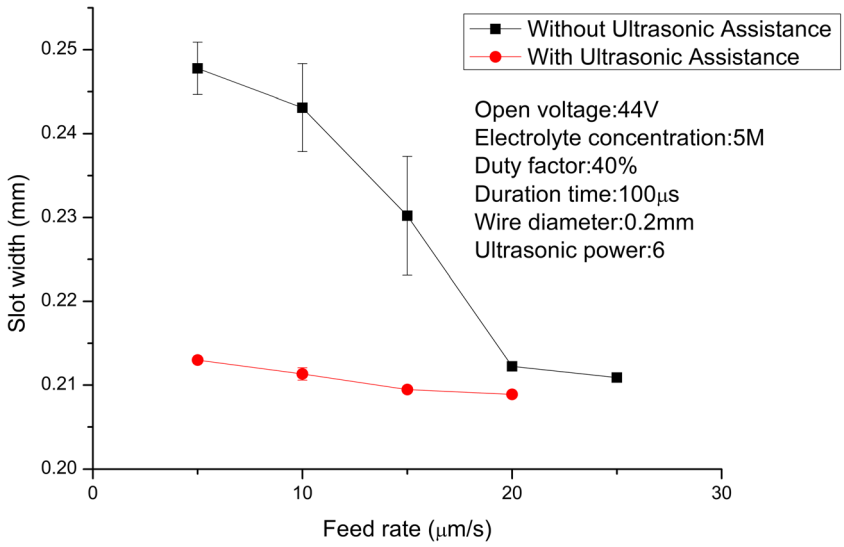

Fig. 19 Schematic of the relationship between feed rate and slot width

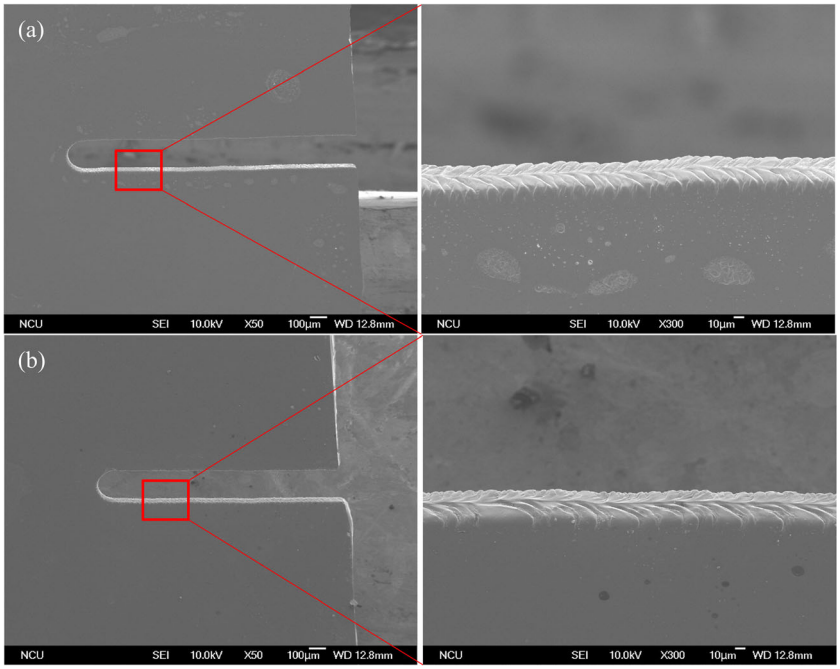

Fig. 20 SEM images of structures processed at various feed rates with ultrasonic assistance (open voltage, 44 V; processing time, 100 μs; duty factor, 40%; and ultrasonic power level, 6): **a** feed rate of 5 μm/s and **b** feed rate of 20 μm/s

power level of 2, and Fig. 22 b displays the SEM image of the fish-bone etching mark processed at a power level 10. Fish-bone etching marks were fewer on the surface of the sidewall processed at the ultrasonic power level of 2 compared with that processed at the ultrasonic power level of 10.

4 Conclusion

This study used ultrasonic-assisted WECDM with continuous electrolyte flow to machine nonconductive quartz wafer. Easy breakage and loss of the wire electrode could be avoided by this method. The machining accuracy and speed can be improved using appropriate WECDM parameters. Relevant results obtained in this study were summarized as follows:

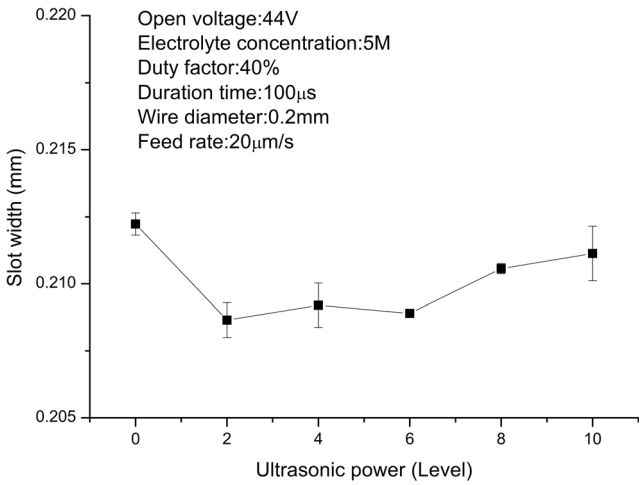

Fig. 21 Schematic of the relationship between ultrasonic power and slot width

1. Ultrasonic vibration considerably affected the gas film. The slot width decreased considerably as the open voltage increased from 38 to 47 V under ultrasonic vibration. Furthermore, the current was relatively stable at an open voltage of 44 V.
2. At all duration times, the slot width in WECDM with ultrasonic assistance was considerably smaller than that in WECDM without ultrasonic assistance. When the processing time was 100 μs, the smallest slot width was 0.222 mm. The surface of the slot sidewalls was vertical and relatively flat.
3. At each duty factor, the slot width obtained in WECDM with ultrasonic assistance was smaller than that obtained in WECDM without ultrasonic assistance. A smaller slot width and stable processing could be achieved at an impact factor of 40%.
4. The slot width decreased as the feed rate increased. The feed rate could only be up to 20 μm/s under ultrasonic assistance.
5. When the experiment was performed without ultrasonic vibration, the slot width was 0.212 mm, which was larger than all other slot widths obtained from the experiments with ultrasonic vibration. Furthermore, the slot width obtained from the experiments with ultrasonic assistance slightly increased with the ultrasonic power increasing.

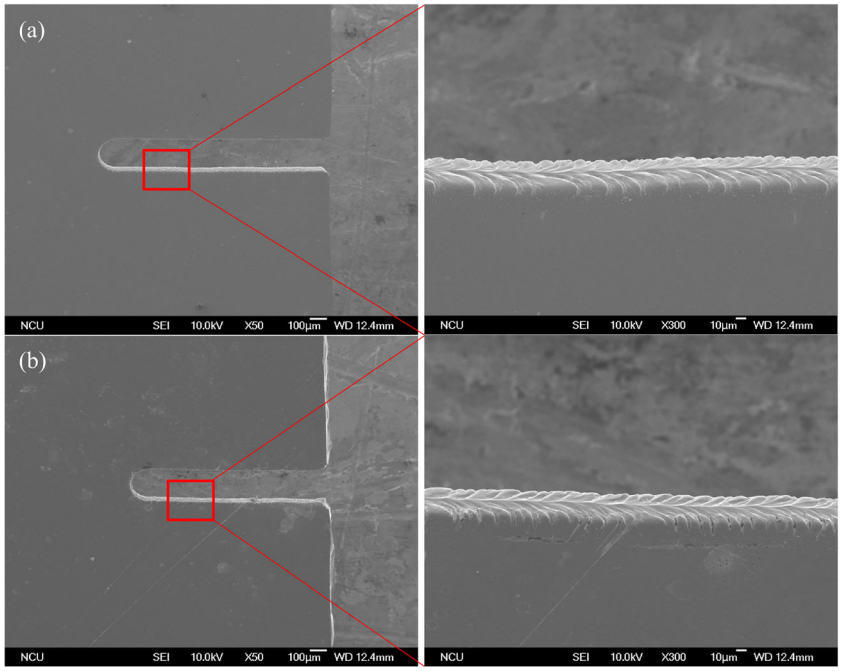

Fig. 22 SEM images of structures processed at various ultrasonic power levels (open voltage, 44 V; duration time, 100 μs; duty factor, 40%; and feed rate, 20 μm/s): **a** level 2 and **b** level 10

6. The smallest slot width was 0.208 mm when the open voltage was 44 V, duration time was 100 μs, duty factor was 40%, feed rate was 20 μm/s, and ultrasonic power level was 2.

Availability of data and material The data and material are available.
Code availability Not applicable for this section.

Author contribution Chun-Hao Yang: conceptualization, methodology, data curation, writing—original draft preparation, visualization, investigation. Hai-Ping Tsui: conceptualization, visualization, investigation, supervision, writing—reviewing and editing.

Declarations

Ethics approval The ethics are approved.

Consent to participate Not applicable for this section.

Consent for publication We consent for publication.

Conflict of interest The authors declare no competing interests.

References

1. Gvozdev AE, Sergeyev NN, Minayev IV, Kolmakov AG, Tikhonova IV, Sergeyev AN, Provotorov DA, Khonelidze DM, Maliy DV, Golyshev IV (2017) Temperature distribution and structure in the heat-affected zone for steel sheets after laser cutting. Inorg Mater Appl Res 8:148–152. https://doi.org/10.1134/S2075113317010178
2. Srivastava M, Tripathi R, Hloch S, Chattopadhyaya S, Dixit AR (2016) Potential of using water jet peening as a surface treatment process for welded joints. Proc Eng 149:472–480. https://doi.org/10.1016/j.proeng.2016.06.694
3. Haghbin N, Ahmadzadeh F, Papini M (2018) Masked microchannel machining in aluminum alloy and borosilicate glass using abrasive water jet micro-machining. J Manuf Process 35:307–316. https://doi.org/10.1016/j.jmapro.2018.08.017
4. Jain VK, Dixit PM, Pandey PM (1999) On the analysis of the electrochemical spark machining process. Int J Mach Tools Manuf 39:165–186. https://doi.org/10.1016/S0890-6955(98)00010-8
5. Bhattacharyya B, Doloi BN, Sorkhel SK (1999) Experimental investigations into electrochemical discharge machining (ECDM) of non-conductive ceramic materials. J Mater Process Technol 95:145–154. https://doi.org/10.1016/S0924-0136(99)00318-0
6. Yang CT, Ho SS, Yan BH (2001) Micro hole machining of borosilicate glass through electrochemical discharge machining (ECDM). KEM 196:149–166. https://doi.org/10.4028/www.scientific.net/KEM.196.149
7. Wüthrich R, Hof LA, Lal A, Fujisaki K, Bleuler H, Mandin P, Picard G (2005) Physical principles and miniaturization of spark assisted chemical engraving (SACE). J Micromech Microeng 15:S268–S275. https://doi.org/10.1088/0960-1317/15/10/S03
8. Wüthrich R, Spaelter U, Bleuler H (2006) The current signal in spark-assisted chemical engraving (SACE): what does it tell us? J Micromech Microeng 16:779–785. https://doi.org/10.1088/0960-1317/16/4/014
9. Mousa M, Allagui A, Ng HD, Wüthrich R (2009) The effect of thermal conductivity of the tool electrode in spark-assisted chemical engraving gravity-feed micro-drilling. J Micromech Microeng 19:015010. https://doi.org/10.1088/0960-1317/19/1/015010
10. Kim D-J, Ahn Y, Lee S-H, Kim Y-K (2006) Voltage pulse frequency and duty ratio effects in an electrochemical discharge microdrilling process of Pyrex glass. Int J Mach Tools Manuf 46:1064–1067. https://doi.org/10.1016/j.ijmachtools.2005.08.011
11. Yang C-K, Cheng C-P, Mai C-C, Cheng Wang A, Hung JC, Yan BH (2010) Effect of surface roughness of tool electrode materials in

ECDM performance. Int J Mach Tools Manuf 50:1088–1096. https://doi.org/10.1016/j.ijmachtools.2010.08.006
12. Yang C-K, Wu K-L, Hung J-C, Lee SM, Lin JC, Yan BH (2011) Enhancement of ECDM efficiency and accuracy by spherical tool electrode. Int J Mach Tools Manuf 51:528–535. https://doi.org/10.1016/j.ijmachtools.2011.03.001
13. Cao XD, Kim BH, Chu CN (2013) Hybrid micromachining of glass using ECDM and micro grinding. Int J Precis Eng Manuf 14:5–10. https://doi.org/10.1007/s12541-013-0001-6
14. Elhami S, Razfar MR (2017) Analytical and experimental study on the integration of ultrasonically vibrated tool into the micro electrochemical discharge drilling. Precis Eng 47:424–433. https://doi.org/10.1016/j.precisioneng.2016.09.015
15. Singh T, Dvivedi A (2018) On performance evaluation of textured tools during micro-channeling with ECDM. J Manuf Process 32:699–713. https://doi.org/10.1016/j.jmapro.2018.03.033
16. Singh T, Dvivedi A (2020) On prolongation of discharge regime during ECDM by titrated flow of electrolyte. Int J Adv Manuf Technol 107:1819–1834. https://doi.org/10.1007/s00170-020-05126-y
17. Peng WY, Liao YS (2004) Study of electrochemical discharge machining technology for slicing non-conductive brittle materials. J Mater Process Technol 149:363–369. https://doi.org/10.1016/j.jmatprotec.2003.11.054
18. Yang CT, Song SL, Yan BH, Huang FY (2006) Improving machining performance of wire electrochemical discharge machining by adding SiC abrasive to electrolyte. Int J Mach Tools Manuf 46:2044–2050. https://doi.org/10.1016/j.ijmachtools.2006.01.006
19. Kuo KY, Wu KL, Yang CK, Yan B-H (2015) Effect of adding SiC powder on surface quality of quartz glass microslit machined by WECDM. Int J Adv Manuf Technol 78:73–83. https://doi.org/10.1007/s00170-014-6602-0
20. Liu JW, Yue TM, Guo ZN (2009) Wire electrochemical discharge machining of Al_2O_3 particle reinforced aluminum alloy 6061. Mater Manuf Process 24:446–453. https://doi.org/10.1080/10426910802714365
21. Manna A, Kundal A (2015) An experimental investigation on fabricated TW-ECSM setup during micro slicing of nonconductive ceramic. Int J Adv Manuf Technol 76:29–37. https://doi.org/10.1007/s00170-013-5145-0
22. Singh A, Jawalkar CS, Vaishya R, Kumar A (2014) A study on wire breakage and parametric efficiency of the wire electro chemical discharge machining process. All India Manufacturing Technology 6
23. Bhuyan BK, Yadava V (2013) Experimental modeling and multi-objective optimization of traveling wire electro-chemical spark machining (TW-ECSM) process. J Mech Sci Technol 27:10
24. Mitra NS, Doloi B, Bhattacharyya B (2015) Predictive analysis of criterial yield during travelling wire electrochemical discharge machining of Hylam based composites. Adv Produc Eng Manag 10:73–86. https://doi.org/10.14743/apem2015.2.193
25. Rattan N, Mulik RS (2017) Improvement in material removal rate (MRR) using magnetic field in TW-ECSM process. Mater Manuf Process 32:101–107. https://doi.org/10.1080/10426914.2016.1176197
26. Rattan N, Mulik RS (2018) Experimental set up to improve machining performance of silicon dioxide (quartz) in magnetic field assisted TW-ECSM process. Silicon 10:2783–2791. https://doi.org/10.1007/s12633-018-9818-z
27. Wang J, Guo YB, Fu C, Jia Z (2018) Surface integrity of alumina machined by electrochemical discharge assisted diamond wire sawing. J Manuf Process 31:96–102. https://doi.org/10.1016/j.jmapro.2017.11.008
28. Wang J, Fu C, Jia Z (2018) Research on oil film-assisted wire electrochemical discharge machining. Int J Adv Manuf Technol 96:2455–2461. https://doi.org/10.1007/s00170-018-1781-8
29. Oza AD, Kumar A, Badheka V, Arora A (2019) Traveling wire electrochemical discharge machining (TW-ECDM) of quartz using zinc coated brass wire: investigations on material removal rate and kerf width characteristics. Silicon 11:2873–2884. https://doi.org/10.1007/s12633-019-0070-y